J Mater Sci (2017) 52:10879–10885

Deactivation of electrically supersaturated Te-doped InGaAs grown by MOCVD

E. L. Kennon[1,*], T. Orzali[2], Y. Xin[3], A. Vert[4], A. G. Lind[1], and K. S. Jones[1]

[1] Department of Materials Science and Engineering, University of Florida, Gainesville, FL 32611, USA
[2] Institute for Compound Semiconductors, Cardiff University, Queen's Buildings, The Parade, Cardiff CF24 3AA, Wales, UK
[3] National High Magnetic Field Laboratory, Florida State University, Tallahassee, FL 32310, USA
[4] Sematech, SUNY Polytechnic Institute, Albany, NY 12203, USA

Received: 3 April 2017
Accepted: 30 May 2017
Published online:
6 June 2017

© Springer Science+Business Media New York 2017

ABSTRACT

Achieving and sustaining the highest doping level possible in InGaAs is critical for the reduction of contact resistance in future microelectronic applications. Tellurium (Te) is a very promising n-type dopant with high reported *n*-type doping densities. However, the stability of this dopant during post-growth thermal processing is unknown. Supersaturated Te-doped InGaAs layers were grown by MOCVD at 500 °C. The electrically active concentration of Te doping was 4.4×10^{19} cm^{-3} as grown. The thermal stability of the Te was investigated by studying the effect of post-growth annealing between 550 and 700 °C on the electrical activation. At all temperatures, the electrical activation decreased from its starting electron concentration of 4.4×10^{19} cm^{-3} down to 6–7 $\times$ 10^{18} cm^{-3}. The rate of deactivation was measured at each temperature, and the activation energy for the deactivation process was determined to be 2.6 eV. The deactivation could be caused by either Te–Te clustering or a Te-point defect reaction. HAADF-STEM images showed no visible clustering or precipitation after deactivation. Based on previous ab initio calculations that suggest the V_{III} population increases as the Fermi level moves toward the conduction band, it is proposed that formation of isolated point defect complexes, possibly a Te–V_{III} complex, is associated with the deactivation process.

Introduction

III–V materials, and particularly InGaAs, are of interest for future integration into CMOS devices because of their higher carrier injection velocities in ballistic short channel devices [1]. This can allow for high speed devices with lower power dissipation. However, with these high-performance devices, the contact resistances to the source and drain can become a significant portion of the device resistance, limiting the drive current and on/off ratio of the device [2]. The International Technology Roadmap for Semiconductors (ITRS) has predicted that contact resistivities less than 1×10^{-8} Ω cm^2 are necessary

Address correspondence to E-mail: elkennon@ufl.edu

DOI 10.1007/s10853-017-1254-8

for future devices [3]. This resistance can be lowered by increasing the doping in the semiconductor just below the metal contact, increasing the number of carriers near the metal–semiconductor interface. A carrier concentration above 6×10^{19} cm^{-3} should be sufficient to achieve a useable contact resistivity [4].

Electrical activation of implanted species is limited to an equilibrium value at the temperature of the activating anneal and is lower in concentration than is useful for desired contact resistivities [5–7]. Silicon is a common dopant in InGaAs, and sufficient concentrations have been grown by molecular beam epitaxy (MBE) to achieve low contact resistances [4, 8]. However, given the low throughput of MBE, this is impractical for industry. Furthermore, these doping levels are supersaturated and deactivate upon subsequent thermal anneal to the same concentration that limits ion implantation [9]. This suggests that the heavily doped layers would potentially deactivate under the thermal budget required during subsequent processing. Metal organic chemical vapor deposition (MOCVD) is a higher throughput technology, but has struggled to reach active carrier concentrations similar to MBE [4, 10, 11]. However, a high active doping concentration of 8×10^{19} cm^{-3} was recently reported for tellurium doping in InGaAs grown by MOCVD [10]. Doping by MOCVD is promising for widespread adoption, but the lower equilibrium doping levels of Te from methods like ion implantation call into question the stability of these heavy doping levels [7]. This paper investigates the thermal stability of MOCVD grown Te-doped InGaAs at these higher concentrations to better assess if this is a viable alternative to Si doping.

Materials and methods

Two samples were grown by MOCVD with the same underlying buffer layer structure as Orzali et al. [10]. This consisted of a Si wafer on which approximately 350 nm of GaAs, 800 nm of InP, and 300 nm of InAlAs were deposited. The InAlAs served as a semi-insulating barrier layer to enable accurate Hall effect measurements. The first sample's $In_{.53}Ga_{.47}As$ layer consisted of 500 nm of InGaAs grown at 600 °C and 100 nm of heavily Te-doped InGaAs grown at 500 °C. The InGaAs layer on the second sample was 600 nm grown at 600 °C and did not have the Te-doped layer, and thus served as a control for the carrier concentration of the background InGaAs. Both samples were grown at 500 °C with pressure at 100 mbar, trimethylgallium, trimethylindium, and arsine fluxes of 275, 113, and 8530 μmol min^{-1}, respectively. Diethyltelluride at a flux of 0.13 μmol min^{-1} was added in the Te-doped layer. This yielded a growth rate of 2.2 μm h^{-1}, so the Te-doped layer was only exposed to 2.7 min at 500 °C during growth.

These wafers were cleaved into squares 1 cm on a side. The pieces were then covered by an atomic layer deposition (ALD) Al_2O_3 layer of 15 nm to protect the InGaAs from degradation during anneals. The deposition was carried out at 250 °C in exposure mode to reduce the incidence of pinholes in the resulting protective cap. The capped samples were annealed via rapid thermal anneal (RTA) and furnace anneals across a range of temperatures from 550 to 700 °C at times appropriate to capture the deactivation of the heavily doped Te layer. Anneals at 550–600 °C were 5 min or greater and carried out entirely in the furnace. Anneals at 700 °C were less than 2 min and entirely RTA. Anneals at 625–650 °C crossed through both RTA and furnace time scales, so an overlap of one point at 5 min with both anneal methods was used to confirm that they achieved similar results. The heavily Te-doped samples were annealed side by side with the undoped samples in order to confirm that there was no variation in measured sheet carrier concentration that was not caused by the deactivation of the Te layer. Post-anneal, the Al_2O_3 cap was removed by a buffered oxide etch (BOE) for 5 min at room temperature. Indium contacts were pressed onto the corners of the samples in a Van der Pauw pattern for Hall effect measurements taken at room temperature.

Cross-sectional transmission electron microscopy (XTEM) was used to confirm layer thicknesses, and high-angle annular dark field scanning transmission electron microscopy (HAADF-STEM) on an aberration corrected JEOL JEM-ARM 200cF TEM was used to look for precipitation of Te after the deactivating anneals. SIMS measurements were taken on a PHI Adept 1010 Dynamic SIMS system using a 20 nA 3 kV Cs+ primary beam while detecting negatively charged secondary ions. There was no sample bias and a 10% detection area over a 500-μm square raster. A similar MOCVD grown sample with a known Te concentration was used for SIMS calibration.

Results

Hall effect measurements were taken on samples before and after annealing to explore the effect of post-growth annealing on the dopant activation/de-activation levels. Hall effect of samples as grown and after being capped with ALD and stripped with BOE was nearly identical, showing that the capping and stripping processes did not alter the activation of the InGaAs layers. A representative deactivation curve of carrier concentration versus anneal time at 700 °C is given in Fig. 1. It is clear that post-growth thermal annealing is inducing a deactivation in the Te dopant. The deactivation of the Te doping follows an exponential decay as indicated by the red line, fit using the function:

$$n = A * e^{-\lambda * t} + C \quad (1)$$

where t is duration of the anneal, n is the electron concentration after any given time, C is the stable doping concentration of 7×10^{18} cm^{-3}, A is the difference between the stable concentration and the initial electron concentration of 4.4×10^{19} cm^{-3}, and λ is the decay constant. The background sheet carrier concentration in the 600 nm undoped InGaAs sample was 4×10^{12} cm^{-2} which was unaffected by anneals compared to 6–7 $\times 10^{13}$ cm^{-2} for the deactivated Te. Thus, even after deactivation, the Te doping level was still more than an order of magnitude above the background doping.

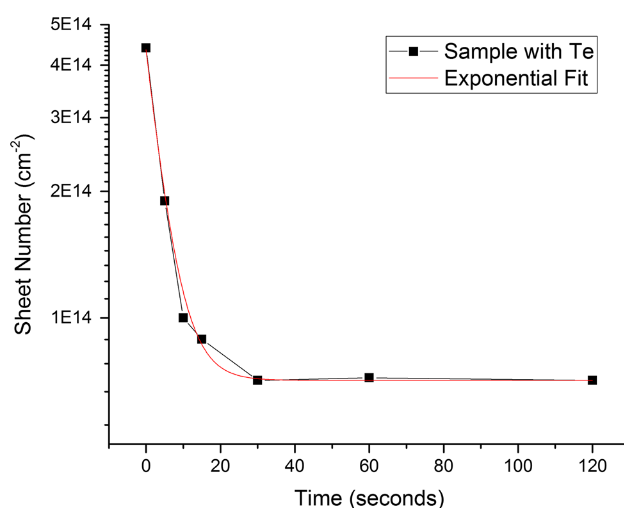

Figure 1 Hall effect data for a time series of anneals at 700 °C showing the deactivation of Te from 4.4×10^{14} to 7×10^{13} cm^{-2}. The *smooth line* represents an exponential fit of the data to extract a deactivation rate.

In order to convert the Hall effect sheet carrier concentrations to electrically active volumetric dopant concentrations it is critical to know how much diffusion is occurring upon annealing. SIMS shown in Fig. 2 indicates an abrupt box Te profile as grown at a concentration of 6.3×10^{19} cm^{-3} which reveals that 70% of the Te is electrically active prior to annealing. After a 700 °C anneal of 2 min, no significant diffusion of the Te profile was observed. As the Te deactivates to a stable level after only 30 s at 700C, it is still valid to divide the sheet number over the depth of the box-like profile, yielding a concentration of 7×10^{18} cm^{-3}. With such a low diffusivity, it is safe to assume that there is a negligible diffusion effect on carrier concentrations during deactivation for the times and temperatures studied.

In an effort to understand diffusion better, Te was also profiled after a much longer anneal of 4 h at 700 °C. The profile looks like typical Fickian diffusion. Hall effect after 4 h yields an active Te sheet number of 8.4×10^{13} cm^{-2}. Applying this sheet number to the diffused profile yields a deactivated value of 7×10^{18} cm^{-3}. The is the same value as was observed after 30 s indicating there is no further deactivation upon extended annealing.

Cross-sectional TEM of the structure in Fig. 3a shows the final Te-doped layer is 100 nm, and the total InGaAs layer thickness is about 600 nm. This image was taken after a 700 °C 2 min RTA to deactivate the Te doping, but the samples look the same as grown and after anneal. An interface is visible where the Te doping begins because of the break between the bulk InGaAs growth at 600 °C and the Te-doped layer grown at 500 °C. HAADF-STEM of the sample surface in Fig. 3b does not show any macroscopic precipitates or incoherent phases (pure Te and most alloys with Ga, In, or As are hexagonal or monoclinic) after deactivation of the Te doping to an equilibrium level as indicated by Hall effect.

Figure 4 compares the effect of deactivation of the material from this study, with a Te concentration of 6.3×10^{19} cm^{-3} and a carrier concentration of 4.4×10^{19} cm^{-3}, to the material grown by Orzali et al. [10] with a Te concentration of 5.5×10^{20} cm^{-3} and a carrier concentration by our measurements of 6.3×10^{19} cm^{-3}. The deactivation proceeds at a similar rate when comparing 10 min furnace anneals at varying temperature. The similar rates indicate that the deactivation is not affected by the difference in Te concentration.

The effect of annealing at additional temperatures between 550 and 700 °C was then investigated. Figure 5 shows that the rate of deactivation is very temperature dependent with deactivation progressing more quickly at higher temperatures as expected. In addition, it is interesting that independent of temperature, the Te deactivates to the same concentration of around 6–7 × 10^{18} cm^{-3}.

To gain insight into the energetics of the deactivation process, the Hall effect decay curves from each temperature were fit with an exponential decay function demonstrated by Eq. (1) and the line in Fig. 1. The decay constants from these curves were plotted according to an Arrhenius relationship as shown in Fig. 6. These points form a line that corresponds to an activation energy of 2.6 eV, which represents the activation energy for the rate limiting step in the Te deactivation process.

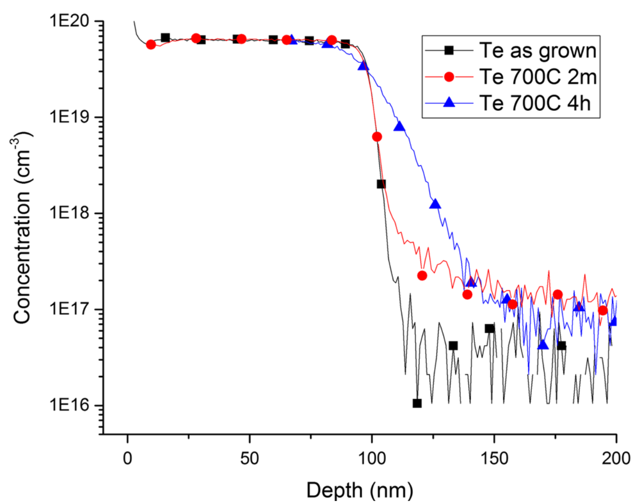

Figure 2 SIMS showing the beginning Te physical concentration and the degree of diffusion after deactivation at 700 °C for 2 min and after 4 h. There is no apparent diffusion after 2 min and Fickian diffusion after 4 h.

Discussion

Tellurium could be deactivating through a variety of mechanisms including precipitation and clustering, which could form a number of point defect combinations. The activation energy derived from Fig. 6 could correspond any of these mechanisms. This work starts the process of narrowing down what could be responsible for Te deactivation.

No large clusters or incoherent precipitates were observed in the HAADF-STEM images or by TEM imaging in Fig. 3. However, the atomic number difference between Te and In in the matrix is fairly small, so it is difficult to discern any clusters of Te in the InGaAs matrix. Small clusters of only a few Te atoms or complexes of a Te atom with another point defect could be responsible for deactivation without being visible by TEM. For this reason, we must look to the diffusion of Te to rule out Te clustering.

The diffusion of Te seen in SIMS is not apparent in the short anneal times comparable to the times observed for deactivation. The diffusion coefficient of Te is known to be small in GaAs and InAs [12, 13] and by annealing for longer time scales, we find that the Te diffusion coefficient in InGaAs falls between them. FLOOPS [14] simulations to match the SIMS

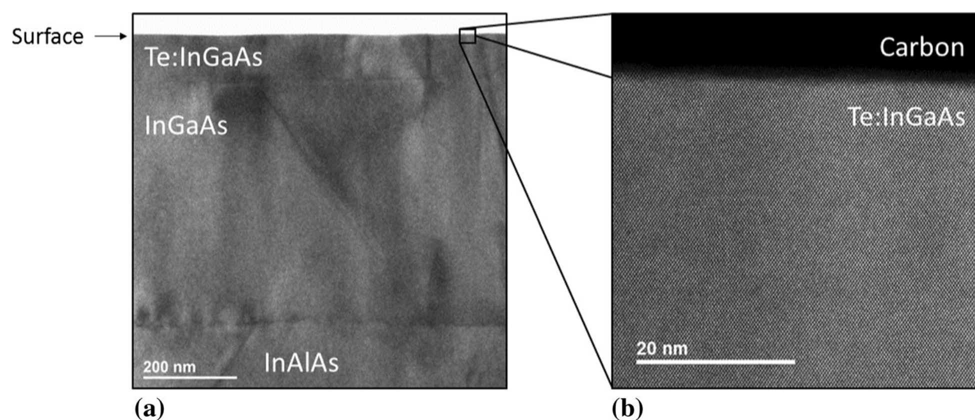

Figure 3 XTEM of InGaAs structure **a** after 700 °C 2 min anneal showing 100 nm of Te:InGaAs on *top*, 500 nm of additional InGaAs and the InAlAs layer at the end of the buffer structure on *bottom*. The clarity of the interfaces is the same as the appearance as grown. **b** HAADF-STEM of the same sample on an aberration corrected TEM looking at the Te-doped layer, where no large precipitates of Te are visible.

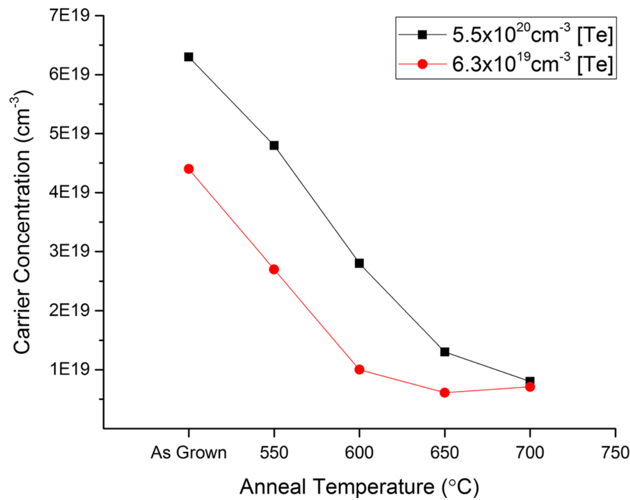

Figure 4 Deactivation during 10 min furnace anneals with varying temperatures progress at the same rate with physical Te concentrations that vary by almost an order of magnitude. This rules out the possibility of a Te diffusion limited deactivation mechanism.

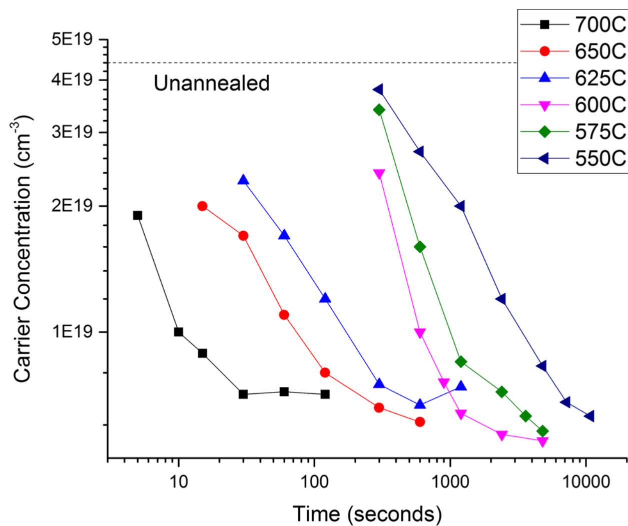

Figure 5 Deactivation curves for all anneal temperatures on a log time plot with the trend for higher temperature anneals to deactivate more quickly. The *dotted line* represents the starting carrier concentration for all samples.

profile of the Te diffusion after 4 h show the diffusivity at 700 °C is approximately 3.6×10^{-17} cm^2 s^{-1}.

Using the diffusivity of Te at 700 °C, the characteristic diffusion length at 30 s (the first point at which the Te is deactivated to an equilibrium value) is 0.66 nm. For our material with a peak Te concentration of 6.3×10^{19} cm^{-3} and assuming a uniform distribution, the average distance between Te atoms in the InGaAs is 2.5 nm. This means that in the time scale where deactivation is occurring, two Te atoms are unlikely to diffuse far enough meet, and certainly not enough would do so for electrical activation to drop by a factor of 5. When comparing to a higher doped sample in Fig. 4, the matching rates of deactivation further support this, since a Te–Te complex would form more readily if the Te atoms started closer together.

From a fundamental point of view, the compressive strain and positive charge of ionized Te atoms would act to repel nearby Te atoms, aligning with the evidence above. In heavily *n*-type doped samples of GaAs with a high Fermi level, ab initio calculations have shown that group III vacancies are more energetically stable than other point defects [15, 16]. These vacancies are negatively charged and would relieve the strain of a Te on an As site, so it makes sense that a group III vacancy clustered to Te is most likely to contribute to the deactivation. DFT calculations to determine the preferred deactivation route of Te are in progress and will be reported in the future.

Although the deactivation progresses to a similar carrier concentration of 6–7 $\times$ 10^{18} cm^{-3} across all temperatures studied, the stable level trends slightly toward the higher end of that range at the higher anneal temperatures. The effect is very minor relative to the normal increase in electrical solubility with increasing temperature observed in other systems [17, 18]. These equilibrium solubility levels after deactivation are also significantly lower than stable activation levels for other dopants in InGaAs, such as Si [9] which deactivates to 1.5×10^{19} cm^{-3}.

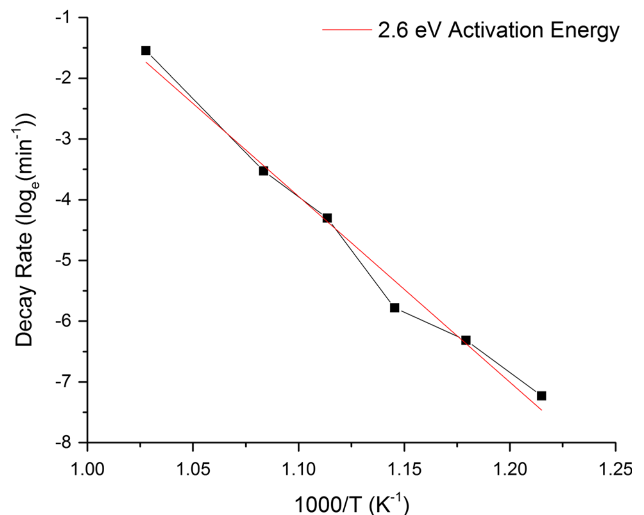

Figure 6 Arrhenius plot of electrical deactivation time constants over all anneal temperatures, showing an activation energy for the deactivation mechanism of 2.6 eV.

Therefore, despite having a more promising as grown *n*-type electrical activation than Si in InGaAs, the final deactivated concentration is half of the Si value so it will be even more important to limit the post-growth thermal processing for Te-doped InGaAs.

Conclusions

The deactivation of heavily doped, electrically supersaturated Te doping in InGaAs was studied for a range of temperatures from 550 °C to 700 °C. The Te doping is found to deactivate from 4.4×10^{19} to $6–7 \times 10^{18}$ cm^{-3} for all temperatures studied. The rate of deactivation was measured, and from this an activation energy of 2.6 eV was determined for the rate limiting step of the deactivation process. HAADF-STEM and other TEM studies did not show any macroscopic precipitate formation suggesting that submicroscopic clusters or point defect complex formation may be responsible for the deactivation. A group III vacancy–Te complex seems to be the most likely candidate for deactivation. The instability of Te to post-growth thermal processing and the lower equilibrium activated value will require care if it is to be adopted in future microelectronic devices.

Acknowledgements

The authors would like to acknowledge Applied Materials for project funding, the Major Analytical Instrumentation Center and Nanoscale Research Facility at University of Florida, the National High Magnetic Field Laboratory at Florida State University (DMR-1157490), and Mikhail Klimov and the Advanced Materials Processing and Analysis Center-Materials Characterization Facility at the University of Central Florida.

Compliance with ethical standards

Conflict of interest The authors declare that we have no conflicts of interest.

References

[1] del Alamo JA (2011) Nanometre-scale electronics with III–V compound semiconductors. Nature 479:317–323. doi:10.1038/nature10677

[2] 2013 International Technology Roadmap for Semiconductors (ITRS). http://www.itrs2.net/2013-itrs.html. Accessed 22 Feb 2015

[3] 2011 International Technology Roadmap for Semiconductors (ITRS). http://www.itrs2.net/2011-itrs.html. Accessed 21 Jun 2016

[4] Baraskar A, Gossard AC, Rodwell MJW (2013) Lower limits to metal-semiconductor contact resistance: theoretical models and experimental data. J Appl Phys 114:154516. doi:10.1063/1.4826205

[5] Pearton SJ (1993) Ion implantation in III–V semiconductor technology. Int J Mod Phys B 7:4687–4761

[6] Lind AG, Rudawski NG, Vito NJ et al (2013) Maximizing electrical activation of ion-implanted Si in In0.53Ga0.47As. Appl Phys Lett 103:232102. doi:10.1063/1.4835097

[7] Gwilliam RM, Anjum M, Sealy BJ et al (1996) Electrical characterisation of magnesium and tellurium implanted indium gallium arsenide. In: Proceedings of 11th international conference on ion implantation Technology, pp 702–704

[8] Dormaier R, Mohney SE (2012) Factors controlling the resistance of Ohmic contacts to n-InGaAs. J Vac Sci Technol B 30:31209. doi:10.1116/1.4705730

[9] Lind AG, Aldridge HL Jr, Bomberger CC et al (2015) Comparison of thermal annealing effects on electrical activation of MBE grown and ion implant Si-doped In0.53Ga0.47As. J Vac Sci Technol B 33:21206. doi:10.1116/1.4914319

[10] Orzali T, Vert A, Lee RTP et al (2015) Heavily tellurium doped n-type InGaAs grown by MOCVD on 300 mm Si wafers. J Cryst Growth 426:243–247. doi:10.1016/j.jcrysgro.2015.05.007

[11] Jiang L, Lin T, Wei X et al (2004) Effects of V/III ratio on InGaAs and InP grown at low temperature by LP-MOCVD. J Cryst Growth 260:23–27. doi:10.1016/j.jcrysgro.2003.08.013

[12] Karelina TA, Lavrishchev TT, Prikhod'ko GL, Khludkov SS (1974) Diffusion of tellurium in GaAs. Izv Akad Nauk SSSR Neorganicheskie Mater 10:228–230

[13] Willardson RK, Goering HL (1962) Compound semiconductors, volume 1, preparation of III-V compounds. Reinhold Pub. Corp., New York

[14] Law ME (1993) FLOODS/FLOOPS manual. Univ. Fla., Florida

[15] Walukiewicz W (1988) Mechanism of Fermi-level stabilization in semiconductors. Phys Rev B 37:4760–4763. doi:10.1103/PhysRevB.37.4760

[16] Northrup JE, Zhang SB (1993) Dopant and defect energetics: Si in GaAs. Phys Rev B 47:6791–6794. doi:10.1103/PhysRevB.47.6791

[17] Hurle DTJ (2010) A thermodynamic analysis of native point defect and dopant solubilities in zinc-blende III–V semiconductors. J Appl Phys 107:121301. doi:10.1063/1.3386412

[18] Eisen FH, Welch BM, Müller H et al (1977) Tellurium implantation in GaAs. Solid State Electron 20:219–223. doi:10.1016/0038-1101(77)90187-3